Bacteriorhodopsin based non-magnetic spin filters for biomolecular spintronics

Bacteriorhodopsin based non-magnetic spin filters for biomolecular spintronics

Vaibhav Varade,[1] Tal Markus,[1] Kiran Vankayala,[1] Noga Friedman,[2] Mordechai Sheves,[2] David H. Waldeck,[3] Ron Naaman[1*]

1. Department of Chemical Physics, Weizmann Institute of Science, Rehovot, Israel

2. Department of Organic Chemistry, Weizmann Institute of Science, Rehovot, Israel

3. Department of Chemistry, University of Pittsburgh, Pittsburgh, Pennsylvania 15260, USA

*Email: ron.naaman@weizmann.ac.il

Abstract

We discuss spin injection and spin valves, which are based on organic and biomolecules, that offer the possibility to overcome some of the limitations of solid-state devices, which are based on ferromagnetic metal electrodes. In particular, we discuss spin filtering through bacteriorhodopsin in a solid state biomolecular spin valve that is based on the chirality induced spin selectivity (CISS) effect and shows a magnetoresistance of ~ 2% at room temperature. The device is fabricated using a layer of bacteriorhodopsin (treated with n-octyl-thioglucoside detergent: OTG-bR) that is adsorbed on a cysteamine functionalized gold electrode and capped with a magnesium oxide layer as a tunneling barrier, upon which a Ni top electrode film is placed and used as a spin analyzer. The bR based spin valves show an antisymmetric magnetoresistance response when a magnetic field is applied along the direction of the current flow, whereas they display a positive symmetric magnetoresistance curve when a magnetic field is applied perpendicular to the current direction.

Keywords: *Chirality, magnetoresistance, spintronics, monolayers, bacteriorhodopsin, spin-transport, ferromagnet*

Introduction

Spintronics aims to exploit the electron's spin for mathematical operations, data transfer, and data storage instead of the electron's charge which is used in conventional electronics.[1] In part, its attractiveness arises from its promise to be more energy efficient because spin manipulation could require much less energy than the charging of capacitors.[2] Any spintronic device requires spin injection into non-magnetic materials and a means to change the conduction through the device by external control. The spin states of electrons are typically manipulated by external magnetic fields and ferromagnetic materials. For example, a Giant Magnetoresistance (GMR) or a Tunneling Magnetoresistance (TMR) based spin valve consists of two ferromagnetic (FM) layers that are separated by a thin non-magnetic layer (metal or insulator); one FM layer is the fixed layer and acts as a polarizer, while the other FM layer changes its transmission axis in the magnetic field and acts as an analyzer for the spins.[3,4]

Spintronic devices are already being used for the spin valve in read heads of hard disks, which operate on the GMR and/or TMR effect.[5,6] Despite the success of these devices and their commercial application, they suffer from intrinsic drawbacks that limit their future development. The first drawback is their limited promise for miniaturization. Because ferromagnetic materials tend to become super-paramagnetic at small (nanometer) sizes, such devices are likely to be limited to areas of about 70 nm^2. There is much effort to solve the problem by converting the devices from being magnetized in plane to being magnetized perpendicular to the film's surface; nevertheless, shrinking the size of the read head in hard disks remains a significant challenge. A second challenge for GMR and TMR devices is the need to have a permanent magnetic film in close proximity

to the free ferromagnetic layer at room temperature.[7] Current technology meets this challenge by using multiple layers of films that stabilizes the permanent magnetic film through antiferromagnetic interactions. Such structures are relatively expensive to produce and they limit the expansion of these memory technologies to devices that are both higher density and lower cost.

The chiral induced spin selectivity (CISS) effect, through which chiral organic molecules act as spin filters, has paved the way to inject spin currents without the use of a ferromagnetic material. A description of the effect, a theoretical model, and the application of the effect in spintronics were published recently.[8] The CISS effect occurs in chiral molecules and arises from a coupling between the spin and the linear momentum of an electron via the chiral electrostatic potential of the molecule. As a result, a chiral molecule transmits mainly one preferred spin.[9,10] Indeed, a high spin polarization has been demonstrated for electrons transmitted through self-assembled monolayers (SAMs) of chiral molecules, such as DNA,[11-14] oligopeptides,[15,16] bacteriorhodopsin,[17] etc. Because of their weak spin-orbit coupling and weak hyperfine interactions, the electron spin lifetime in organic molecules is long and organic molecules are considered as passive elements in spin transport processes.[18-23] The CISS effect indicates that chiral organic molecules are not passive elements, rather they can act as spin filters.[24]

In the last few years, the CISS effect has been shown to manifest itself in several phenomena, including spin-dependent electrochemistry,[25,26] spin selectivity in photoelectrochemical water splitting,[27-29] spin-dependent photoluminescence,[30] spin transport in chiral quantum dots,[31,32] and in non-magnetic spin injection.[33] The magnetoresistance of a GMR or TMR based spin valve (see Fig. 1(a)) varies according to

the magnetization direction of the layers and its response is symmetric as a function of magnetic field direction; see Fig. 1(d). In contrast, a CISS based spin valve replaces the ferromagnetic reference layer and the insulating barrier with a chiral tunneling barrier; see Fig. 1. A chiral tunneling barrier may consist of one uniform layer or can be a chiral ultrathin barrier that is overcoated with an achiral insulating layer to block any leakage current. Chiral tunneling barriers have been comprised of chiral molecules (e.g., oligopeptide, L/D-cysteine,[33] helicenes[34]), chiral nanoparticles (e.g., CdSe quantum dots[31]), chiral metal oxide films (SAM/Al_2O_3),[33] or other materials.[35] Successful injection of a spin polarized current has been demonstrated for these tunneling barriers by using the top FM layer as an analyzer for the spin polarization. For a CISS-based spin filter, an antisymmetric magnetoresistance response is observed because the applied magnetic field does not change the molecules' chirality, hence the filtered spin polarization.[8] The magnetoresistance in CISS based spin valves has been observed to vary from 1% to as high as 20% in different chiral systems and does not vary much with temperature. In contrast, conventional GMR/TMR based spin valves display a strong decrease in magnetoresistance with increasing temperature.[36]

The schematic drawing in Fig. 1(b) shows the low and high resistance conditions for the magnetoresistance curve of a CISS-based spin valve. As the external magnetic field is varied from zero, more domains are magnetized in the ferromagnet along the direction of the applied magnetic field. When the magnetic field is applied in parallel to the preferred spin polarization for transmission through the chiral tunnel barrier, a low resistance state exists because the applied magnetic field magnetizes the FM analyzer in the direction of the preferred spins. This state changes to a high resistance state once the magnetic field is

reversed because the magnetization of the analyzer is antiparallel to the spin polarization of the tunneling current from the chiral barrier. The sketch on the right shows schematically the magnetoresistance response of the CISS based device; the magnetoresistance either increases or decreases depending on the spin alignment of the electrons transmitted through the chiral molecules.

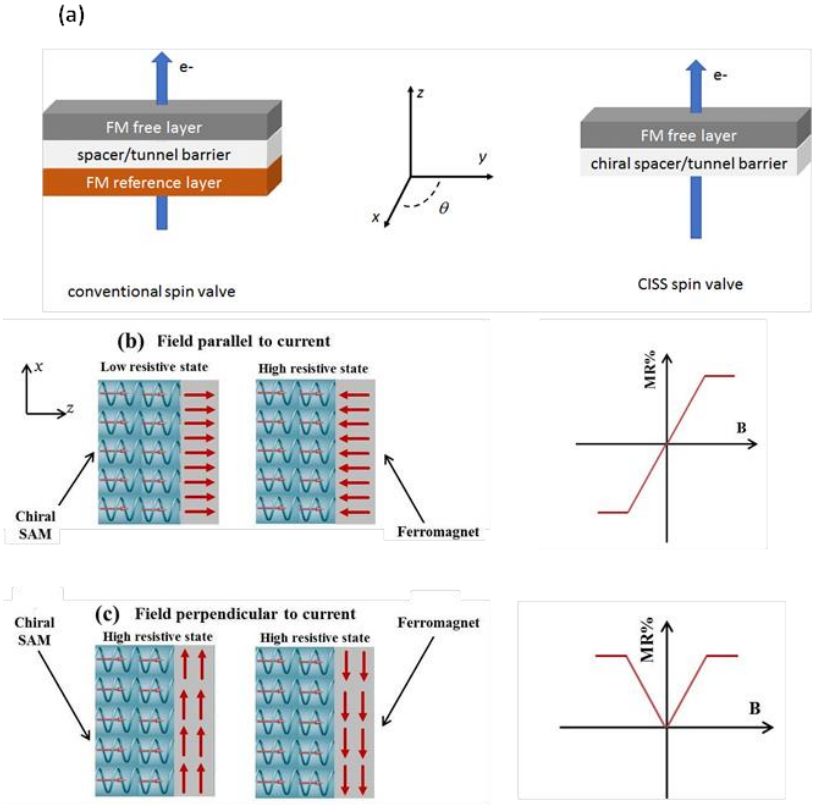

Fig. 1: Panel (a) shows schematic diagrams for the operation of a conventional spin-valve (left) and a CISS-based spin valve (right). Panel (b) depicts the magnetoresistance conditions with the direction of external applied magnetic field in the chiral SAM based spin valves when the magnetic field is parallel to the current direction on the left and the corresponding magnetoresistance curve on the right. Panel (c) depicts situation in which the magnetic field direction is perpendicular to the current direction and shows its corresponding magnetoresistance (MR) response on the right.

The schematic diagram in Fig. 1(c) shows an additional case in which the applied field is directed perpendicular to the direction of current flow. In this geometry, the resistivity for the spin current should not depend on the direction of the magnetic field in

the *xy*-plane because the magnetization domains in the FM will be perpendicular to the spin polarization for both current directions (along *z*). The sketch on the right shows schematically the magnetoresistance response of the CISS based device when the magnetic field is applied perpendicular to the current direction.

The configuration in which the magnetic field is perpendicular to the current has not been studied experimentally for chiral SAM based spin valves. Here we present experimental data for a CISS based TMR device in which all the configurations shown in Fig. 1(b) and 1(c) are studied. These new data are obtained for a monolayer film of the protein bacteriorhodopsin as the tunneling barrier, and their behavior with the applied magnetic field direction demonstrate that they operate via the chiral induced spin selectivity effect, *vide infra*.

A second new feature of this work is the demonstration that a protein, bacteriorhodopsin, film can be used as the spin filtering material in a CISS based spin valve. Bacteriorhodopsin (bR) is a trans-membrane protein, which acts as a light-induced proton pump in the purple membrane (PM) of the archaebacterium *Halobacterium salinarum*. The protein is composed of seven transmembrane helices in which a retinal chromophore is covalently bound to the protein's center. The purple membrane that contains the bR, and the bR itself, have attracted much interest from biophysicists and biophysical chemists because of its interesting optoelectronic and photochromic properties, as well as its long-term stability with regard to thermal, chemical, and photo-induced degradation.[37-40] Most of the studies on bR as an electron transfer component have focused on its photoconductivity and photovoltaic behavior.[41-44] Recent experiments with Mott polarimetry, spin dependent electrochemistry, and magnetic field

controlled photoluminescence in a hybrid system with CdSe nanoparticles have shown that bR purple membranes can filter spins and that it is linked to the integrity of the protein's folded structure.[35,45] We have examined the magnetoresistance of bR-based spin valves for two types of bR, *i.e.,* wild-type (WT) and bR treated with the non-ionic detergent n-octyl-thioglucoside (OTG);[46] however, the performance of the devices with the OTG-bR are much superior and is emphasized in the presentation given below. This difference arises from the better controlled deposition of the bR treated with OTG on the surface, as compared to the WT bR.

Device Production

The protein film characterization: Self-assembled monolayers of OTG-bR were formed on a Au electrode coated with cysteamine, using a procedure like that described earlier.[44] The cysteamine creates a positively charged interface that promotes the adsorption and immobilization of the protein. The adsorbed films OTG-bR were characterized by polarization modulation-infrared reflection absorption spectroscopy (PMIRRAS) and atomic force microscopy (AFM) measurements. Topography images of the bare Au and OTG-bR modified Au substrates show a clear difference in the surface topography between bare and OTG-bR modified Au surfaces, confirming the presence of an OTG-bR monolayer with a thickness of ~ 6 nm; data are provided in Fig. S1 of the supplemental information. The PMIRAS spectra were taken using a ThermoScientific FTIR instrument (Nicolet 6700) equipped with a VariGATR accessory (Harrick Scientific). The spectra were collected by accumulating a minimum of 2000 scans per sample at an 80° angle of incidence and they were analyzed and processed using OMNIC software. Fig. 2(a) shows the IR spectrum for the cysteamine (C_2H_7NS) self-assembled monolayer (SAM)

on gold, and it exhibits a few characteristic peaks such as 1610 cm^{-1} that arise from the N-H bending mode and peaks at 1370 and 1262 cm^{-1} that are attributed to C-H bending vibrations. At higher wavenumber, a weak band corresponding to the N-H stretching mode at 3230 cm^{-1} is evident.

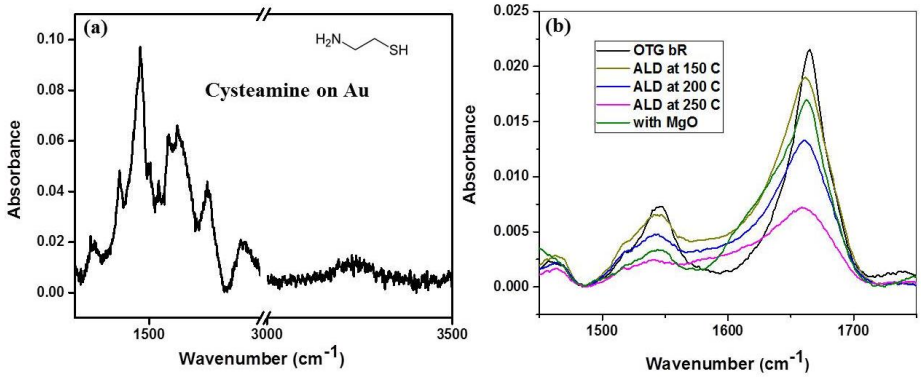

Fig. 2: Polarization modulation-infrared reflection absorption spectra of (a) cysteamine on Au; and (b) OTG-bR, OTG-bR with alumina deposited using ALD at different temperatures, and OTG-bR with MgO on Au surface functionalized with cysteamine.

Once high quality cysteamine/Au surfaces were obtained, the substrates were treated with a buffered solution of OTG-bR which adsorbs electrostatically. Fig. 2(b) shows the IR absorption spectra of the SAM of OTG-bR on Au functionalized with cysteamine in the amide I /amide II spectral region[44] for the Cy/OTG-bR assembly, OTG-bR assemblies covered with different 2.5 nm alumina layers, and a OTG-bR assembly covered with 2.5 nm MgO film. The Cy/OTG-bR assembly shows the characteristic stretching frequency at 1667 cm^{-1}, which corresponds to the amide I band, and a peak at 1544 cm^{-1}, which corresponds to the amide II band. The peak amplitudes are in a ratio of about 3-to-1 for the amide I-to-amide II, which is indicative of the folded protein, and substantiates the formation of OTG-bR protein on the cysteamine/Au surface. The spectra for the Cy/OTG-bR/Al_2O_3 (alumina deposited via ALD at 100 C, 200 C, and 250 C)

display the amide I and amide II bands; however they decrease in amplitude (and amplitude ratio) and broaden at the higher deposition temperatures which are required for reliable tunnel barriers to form. The spectrum of the Cy/OTG-bR/MgO (MgO deposited via e-beam evaporation) shows less degradation as compared to the alumina structures; however, the spectra indicate that the top oxide layer affects the quality of the OTG-bR with an amide I to amide II band intensity ratio of about 5.5-to-1 and about 70 % increase in the peak widths.

Device fabrication and characterization: The oxide deposition affects the performance and limits the reliability of these "sandwich" like protein devices. Only 2% to 3% of the devices that were fabricated with Al_2O_3 barriers were usable, whereas 40% to 50% of those fabricated with MgO barriers were usable. Note that GMR based spin valves, which use e-beam evaporated MgO deposited at ultraslow rates, can serve as an excellent tunnel barrier, as good as radio frequency sputtered MgO.[47] Because of the need to use higher deposition temperatures for the Al_2O_3 barriers, the quality of the protein film was degraded, hence these films were not used in the spin injector studies. See the Supplemental Information for a more detailed discussion.

The SAM/OTG-bR/MgO devices were fabricated with the chiral SAM on a Au electrode as the injector and a ferromagnetic top contact of Ni (150 nm thick) was evaporated onto the MgO as the polarization analyzer. The devices were created in a cross geometry using Au and Ni traces of 1 micron width, patterned by photolithography. The measurements were performed in a four-point probe configuration; see Fig. 3. The magnetoresistance measurements were performed in a Cryogenics cryostat equipped with a superconducting magnet by varying the magnetic field from -1 T to +1 T at different

temperatures down to 20 K. Measurements were performed with a constant current of 1 mA.

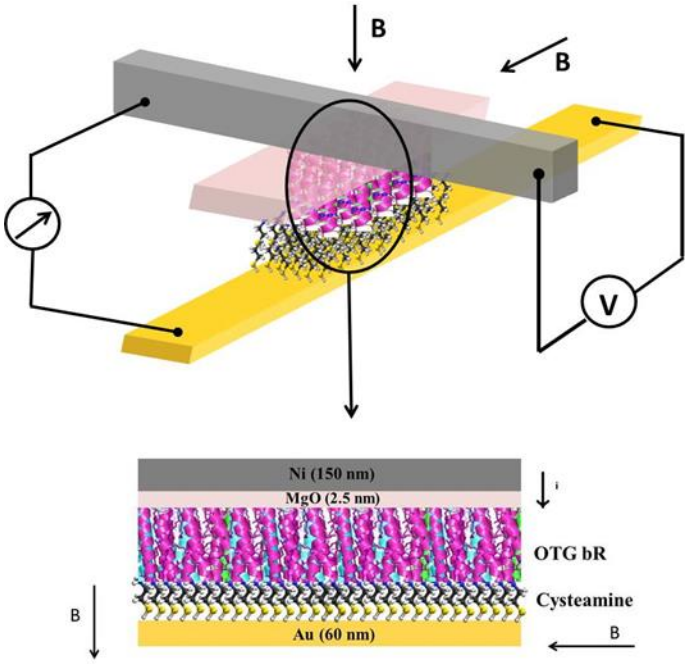

Fig. 3: Typical cross geometry structure of biomolecule protein-based spin valve where B is the applied magnetic field

Results and discussion

Spin valves based on the two types of bR, namely wild-type bR (WT-bR) and octyl-thiolglucoside bR (OTG-bR), were studied. Previous work has shown that chiral induced spin selectivity (CISS) can be observed for WT-bR,[17,45] however no studies have reported CISS for OTG-bR. Functional spin valves could be created by adsorbing WT-bR onto Au electrodes with an MgO barrier, however the WT-bR formed patches on the surface which limited the reproducibility and reliability of these devices. More details on the WT-bR devices is supplied in the supplementary information. Note that the production of

working devices was only about 5% for the Au/WT-bR/MgO/Ni devices. Here we report on the Au/Cy/OTG-bR/MgO/Ni devices.

Fig. 4(a) shows temperature dependent magnetoresistance (MR) measurements as a function of the magnetic field applied parallel (or antiparallel) to the current direction for the Au/Cy/OTG-bR/MgO/Ni devices. Note that the production of working devices was 50-60 %. An antisymmetric MR curve was observed with a net MR as high as ~2 % at room temperature. In contrast to traditional GMR devices which commonly increase their MR with decreasing temperature, the MR for the OTG-bR devices decreased with temperature, to ~0.8 % at 20 K. The decrease in the CISS effect with decreasing temperature was recently observed in several other cases and it is waiting for theoretical explanation. The Au/Cy/OTG-bR/MgO/Ni devices have stronger temperature dependence than other CISS based spin valves. This unusual temperature dependence (a higher MR at higher T) indicates that the chiral OTG-bR plays a role in the spin filtering process and may be linked to conformational change(s) in the protein.[48]

Fig. 4(b) shows the MR curves that were obtained as a function of magnetic field applied in the direction perpendicular to the current flow. The MR effect is found to be

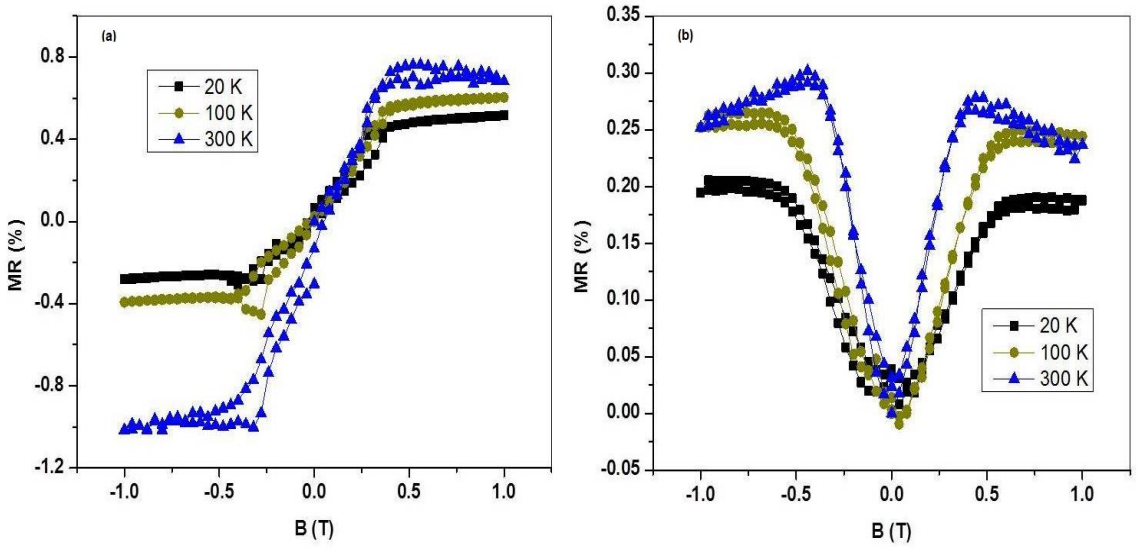

Fig. 4: Magnetoresistance of OTG-bR spin valve as a function of magnetic field when applied to (a) parallel direction to current (b) perpendicular direction to current.

positive and symmetric relative to the direction of the magnetic field. The symmetric shape of these curves, zero at zero-field and increasing to a saturation limit at high field, independent of direction. This shape is symmetric, like that commonly observed for traditional GMR/TMR devices. These results are consistent with spin alignment along the current direction, so that the resistance is not affected by the direction of the magnetization perpendicular to it. The increased resistance at high field was previously observed for organic molecules.[21]

To further confirm the results, control experiments with spin valves that do not contain OTG-bR; i.e., Au/SAM/MgO/Ni, were performed. Fig. 5 compares the MR data for spin valves with and without OTG-bR as a function of magnetic field, at room temperature. The devices which contain the protein show a large, circa 1.8 %, MR change whereas the devices without the protein have a near zero MR response at positive fields and a slightly negative, -0.25%, response at negative fields. The asymmetry in the absolute value of the MR at the positive and negative fields may arise from the inhomogeneity of the ferromagnetic layer making the magnetic anisotropy to favor one spin.

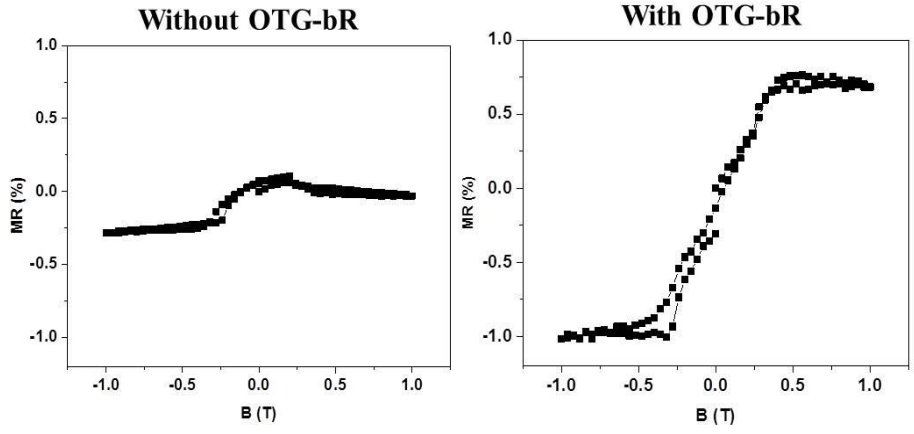

Fig. 5: Magnetoresistance data for spin valves without OTG-bR (left panel) and with OTG-bR (right panel) when a magnetic field is applied parallel to the current.

Conclusion

We have successfully demonstrated the construction of a protein-based solid-state spin valve. By attaching the purple membrane through a self-assembled monolayer of linker (cysteamine) and by using low temperature deposition of an MgO layer, we were able to achieve a relatively high yield of working devices (*ca* 50%). The MR measured with these devices is about 2 % at room temperature and the MR curve is antisymmetric with respect to the direction of magnetic field, when it is applied along the current direction. This latter feature is a signature of spin filters that operate on the CISS principle. When the magnetic field is applied perpendicular to the current, symmetric MR curves are obtained similar to the behavior that is known for achiral organic films. The reduction of the MR values at lower temperature, may be related to conformational changes in the proteins, however it awaits a theoretical explanation.

It is shown here that the effect of magnetic field on the spin transport through the protein is not isotropic and depends on the relative orientation between the magnetic field and the electron trajectory. This data provide a new insight on the magnetic effect in proteins which was not addressed before.

Because CISS based spin filtering does not require a permanent ferromagnetic layer (as in GMR/TMR based spin valves), it allows for miniaturization, in principle, to the size of the spin filtering element, i.e., a single molecule. Hence, the spin valve concept discussed here allows for reducing the sizes of read heads of hard disks, as well as the further miniaturization of magnetic memory elements.

Acknowledgements

This research was partially supported by the Israel Science Foundation, by the European Research Council under the European Union's Seventh Framework Program (FP7/2007-2013)/ERC grant agreement n° 338720 CISS, and by the John Templeton Foundation. VV thanks Dr. Anup Kumar for his supportive help in lab. DHW acknowledges support from the US National Science Foundation (CHE 1464701).

References

1 I. Zutic, J. Fabian and S. D. Sarma, *Rev. Mod. Phys*., 2004, **76**, 323-410.

2 S. Bandyopadhyay and M. Cahay, *Nanotechnology*, 2009, **20** 412001.

3 E. Y. Tsymbal and D. G. Pettifor, *Solid State Phys.*, 2001, **56**, 113–237.

4 Y. M. Lee, J. Hayakawa, S. Ikeda, F. Matsukura and H. Ohno, *Appl. Phys. Lett.*, 2007, **90**, 212507.

5 C. Chappert, A. Fert and F. N. Van Dau, *Nat. Mater*., 2007, **6**, 813-823.

6 A. Fert, *Rev. Mod. Phys*., 2008, **80**, 1517-1530.

7 T. Miyazaki and N Tezuka, *J. Magn. Magn. Mater.*, 1995, **139** L231.

8 K. Michaeli, V. Varade, R. Naaman and D. H. Waldeck, *J. Phys. Condens. Matter*, 2017, **29**, 103002

9 R. Naaman, D. H. Waldeck, *J. Phys. Chem. Lett.*, 2012, **3**, 2178–2187.

10 K. Michaeli, N. Kantor-Uriel, R. Naaman and D. H. Waldeck, *Chem. Soc. Rev.*, 2016, **38**, 188–229.

11 B. Gohler, V. Hamelbeck, T. Z. Markus, M. Kettner, G. F. Hanne, Z. Vager, R. Naaman and H. Zacharias, *Science*, 2011, **331**, 894.

12 Z. Xie, T. Z. Markus, S. R. Cohen, Z. Vager, R. Gutierrez and R. Naaman, *Nano Lett.*, 2011, **11**, 4652–4655.

13 T. J. Zwang, S. Hürlimann, M. G. Hill and J. K. Barton, *J. Am. Chem. Soc.*, 2016, **138**, 15551–15554.

14 J. M. Abendroth, N. Nakatsuka, M. Ye, D. Kim, E. E. Fullerton, A. M. Andrews and P. S. Weiss, *ACS Nano*, 2017, **11**, 7516–7526.

15 M. Kettner, B. Göhler, H. Zacharias, D. Mishra, V. Kiran, R. Naaman, C. Fontanesi, D. H. Waldeck, S. Sek, J. Pawowski and J. Juhaniewicz, *J. Phys. Chem. C*, 2015, **119**, 14542–14547.

16 A. C. Aragonès, E. Medina, M. Ferrer-Huerta, N. Gimeno, M. Teixidó, J. L. Palma, N. Tao, J. M. Ugalde, E. Giralt, I. Díez-Pérez, V. Mujica, *Small* 2017, **13**, 1602519.

17 D. Mishra, T. Z. Markus, R. Naaman, M. Kettner, B. Göhler and H. Zacharias, *Proc. Natl. Acad. Sci.*, 2013, **110**, 14872–14876.

18 Z. H. Xiong, D. Wu, Z. V. Vardeny and J. Shi, *Nature*, 2004, **427**, 821.

19 D. Sun, E. Ehrenfreund and Z. Valy Vardeny, *Chem. Commun.*, 2014, **50**, 1781–1793.

20 T. S. Santos, J. S. Lee, P. Migdal, I. C. Lekshmi, B. Satpati and J. S. Moodera, *Phys. Rev. Lett.*, 2007, **98**, 16601.

21 W. Wagemans, P. Janssen, A. J. Schellekens, F. L. Bloom, P. A. Bobbert and B. Koopmans, *SPIN*, 2011, **1**, 93–108.

22 M. Gobbi and E. Orgiu, *J. Mater. Chem. C*, 2017, **22**, 2706–2710.

23 W. Wagemans and B. Koopmans, *Phys. Status Solidi B*, 2011, **248**, 1029–1041.

24 R. Naaman and D. H. Waldeck, *Annu. Rev. Phys. Chem.*, 2015, **66**, 263–281.

25 P. C. Mondal, C. Fontanesi, D. H. Waldeck and R. Naaman, *ACS Nano*, 2015, **9**, 3377–3384.

26 P. C. Mondal, C. Fontanesi, D. H. Waldeck and R. Naaman, *Acc. Chem. Res.*, 2016, **49**, 2560–2568.

27 W. Mtangi, V. Kiran, C. Fontanesi and R. Naaman, *J. Phys. Chem. Lett.*, 2015, **6**, 4916–4922.

28 W. Mtangi, F. Tassinari, K. Vankayala, A. V. Jentzsch, B. Adelizzi, A. R. A. Palmans, C. Fontanesi, E. W. Meijer and R. Naaman, *J. Am. Chem. Soc.*, 2017, **139**, 2794–2798.

29 F. Tassinari, K. Banerjee-Ghosh, F. Parenti, K. Vankayala, A. Mucci and R. Naaman, *J. Phys. Chem. A*, 2017, **121**, 15777–15783.

30 P. C. Mondal, P. Roy, D. Kim, E. E. Fullerton, H. Cohen and R. Naaman, *Nano Lett.*, 2016, **16**, 2806–2811.

31 B. P. Bloom, V. Kiran, V. Varade, R. Naaman and D. H. Waldeck, *Nano Lett.*, 2016, **16**, 4583–4589.

32 B. P. Bloom, B. M. Graff, S. Ghosh, D. N. Beratan and D. H. Waldeck, *J. Am. Chem. Soc.*, 2017, **139**, 9038–9043.

33 S. P. Mathew, P. C. Mondal, H. Moshe, Y. Mastai, R. Naaman, *App. Phys. Lett.* 2014 **105**, 242408.

34 V. Kiran, S. P. Mathew, S. R. Cohen, I. H. Delgado, J. Lacour and R. Naaman, *Adv. Mater.*, 2016, **28**, 1957–1962.

35 P. C. Mondal, N. Kantor-Uriel, S. P. Mathew, F. Tassinari, C. Fontanesi, R. Naaman, *Adv. Mat. 2015*, **27**,1924-1927.

36 J. Garcia-Torres, E. Valls and E. Gómez, *J. Magn. Magn. Mater.*, 2010, **322**, 3186–3191.

37 A. V Patil, T. Premaruban, O. Berthoumieu, A. Watts and J. J. Davis, *J. Phys. Chem. B*, 2012, **116**, 683–689.

38 S. Crittenden, S. Howell, R. Reifenberger, J. Hillerbrecht and R. R. Birge, *Nanotechnology*, 2003, **14**, 562–565.

39 A. G. Manoj and K. S. Narayan, *Appl. Phys. Lett.*, 2003, **83**, 3614.

40 T. Jussila, M. Li, N. V. Tkachenko, S. Parkkinen, B. Li, L. Jiang and H. Lemmetyinen, *Biosens. Bioelectron.*, 2002, **17**, 509–515.

41 B. T. He, N. Friedman, D. Cahen, M. Sheves, *Adv. Mater.*, 2005, **17**, 1023–1027.

42 Y. Jin, N. Friedman, M. Sheves, T. He and D. Cahen, *Proc. Natl. Acad. Sci.*, 2006, **103**, 8601.

43 S. Mukhopadhyay, S. R. Cohen, D. Marchak, N. Friedman, I. Pecht, M. Sheves and D. Cahen, *ACS Nano*, 2014, **8**, 7714–7722.

44 S. Mukhopadhyay, W. Ga, D. Cahen and I. Pecht, M. Sheves, *Phys. Chem. Chem. Phys.*, 2016, **18**, 25671–25675.

45 P. Roy, N. Kantor-Uriel, D. Mishra, S. Dutta, N. Friedman, M. Sheves, R. Naaman, *ACS Nano*, 2016, **10**, 4525–4531.

46 N. D. Denkov, H. Yoshimura, T. Kouyama, J. Walz and K. Nagayama, *Biophys. J.*, 1998, **74**, 1409–1420.

47 H. Kurt, K. Oguz, T. Niizeki and J. M. D. Coey, *Appl. Phys. Lett.*, 2010, **107**, 83920.
48 S. Tuzi, A. Naito, H. Saitô, *Eur. J. Biochem*. 1996, **239**, 294-301.

TOC: